ISIJ International, Vol. 47 (2007), No. 10, pp. 1394–1400

Mechanism of Carbothermic Reduction of Hematite in Hematite–Carbon Composite Pellets

Jian YANG, Tomoyuki MORI and Mamoru KUWABARA

Department of Materials, Physics and Energy Engineering, Graduate School of Engineering, Nagoya University, Furo-cho, Chikusa-ku, Nagoya, Aichi 464-8603 Japan.

(*Received on May 7, 2007; accepted on August 7, 2007*)

Isothermal reduction experiments are carried out to study carbothermic reduction of hematite in hematite–graphite composite pellets. The carbothermic reduction is dominated by the direct reduction at the initial stage of reduction, and it is determined by the indirect reduction together with the carbon solution loss reaction when the CO partial pressure exceeds a certain value, which is dependent on the temperature. The reduction is greatly promoted due to the increment of the contact area between the hematite and graphite particles and enhancement of heat conduction in the hematite–graphite composite pellets.

The indirect reduction together with the carbon solution loss reaction is markedly activated with increasing temperature. At a moderate carrier gas flow rate, the carbothermic reduction rate reaches the highest value. The reduction can also be effectively improved with decreasing the graphite particle size.

The relationship of reduction products, heating temperature and holding time has been obtained from the XRD analysis results at the different stages for various temperatures under the present experimental conditions. The SEM observation indicates that the indirect reduction together with the carbon solution loss reaction should dominate the carbothermic reduction of hematite at the later stage of reduction.

KEY WORDS: carbothermic reduction; hematite; composite pellet; reduction product; direct reduction; indirect reduction.

1. Introduction

In recent years, increasing attention has been paid to the carbon composite iron ore agglomerates by many strategists and researchers in ironmaking industry. The coal-containing iron ore agglomerates were used in the direct reduced iron (DRI) process, such as FASTMET[1] and COMET.[2] On the other hand, for improving the blast furnace production and operation flexibility, some researchers have tried to use the carbon composite iron ore agglomerates as the blast furnace burden.

Several new processes using carbon composite iron ore agglomerates were recently developed. High Quality Iron Pebble (Hi-QIP) process may be a new method to produce DRI.[3] By use of the mixture of fine ore and fine carbonaceous material, the separated metal and slag could be obtained in a rotary hearth furnace. The carbon composite iron ore hot briquette was developed for being used in the shaft furnace.[4] Reduction degree reached 95% in about 10 min during the briquette descending to the bottom of heat reserve zone of 1 373 K. Therefore, Utilization of the carbon composite iron ore hot briquette was promising to decrease the fuel rate and the discharging amount of CO_2, and elongate the furnace life. A Sheet Material Inserting Metallization Method (SMIMET),[5] in which a sheet of material consisting of the coal and iron ore mixture was inserted in a rotary hearth furnace, was developed for producing DRI. Over 90% metallization was achieved with the coal ratio up to 20%. The non-spherical carbon composite agglomerates were also tired in a lab-scale manufacture for recycling steel work dust and improving blast furnace performance.[6]

In addition to the new process development, the fundamental studies on the mechanism and kinetics of carbothermic reduction of iron oxide was energetically carried out for the carbon composite iron ore agglomerates. In a simultaneous reaction using a hematite–graphite facing pair, Kashiwaya *et al.*[7] found the starting temperature of gasification decreased from 1 173 to 873 K in the facing pair under CO_2 atmosphere, and to 523 K under CO atmosphere due to the coupling phenomenon of reduction and gasification. Iguchi *et al.* made systematical studies on reduction mechanism in carbon composite iron ore pellet. The reaction model was proposed,[8] and the reaction mechanism, swelling rate and crushing strength of pellet were investigated[9] in oxygen bearing gas flow. Rate of direct reduction[10] was measured in vacuum, and kinetics of the reactions[11] was studied from vacuum to 0.1 MPa. Additionally, for the carbon composite iron ore agglomerates, a great deal of research was done on the reduction and melting behavior,[12–16] effects of the carbon content[17] and the atmospheric gas composition[18] on the reduction behavior, the cold strength enhancement mechanism,[19] the mechanism of pig iron making from magnetite ore pellets containing coal

at low temperature[20] and by microwave heating.[21]

Furthermore, great attention has been paid to mechanical milling of iron oxide and carbonaceous material in recent years. It was found that the mixing state and the structure of composite significantly influenced reduction kinetics. The temperature of reduction and carbon gasification was remarkably decreased with mixed-grinding of iron oxides and carbonaceous materials.[22,23] Gas evolution during the mechanical milling was analyzed.[24] The concepts of nano-reactor[25] and a strong contact situation[26] were proposed to explain the enhancement of reduction and gasification by mechanical milling of the carbon and iron oxide mixture. The reduction kinetics of hematite powder mechanically milled with graphite was also studied.[27] However, further investigation is necessary to clarify the effects of the gas mixture around the closely arranged iron ore and carbonaceous material particles, and exceedingly increased specific surface area on the reduction rate of hematite.

In the present study, hematite–graphite composite pellets are manufactured by use of a cold isostatic press (CIP). By use of the isothermal reduction method, effects of temperature, carrier gas flow rate, graphite particle size on the carbothermic reduction rate of hematite are investigated experimentally. The pellets after reduction are observed by use of SEM and optical microscope. The changes in the compositions of the reduced pellets at the different stages of reduction are qualitatively measured using XRD patterns. The possible existence regions of the different reduction products are determined at the different stages of reduction for various temperatures under the present experimental conditions.

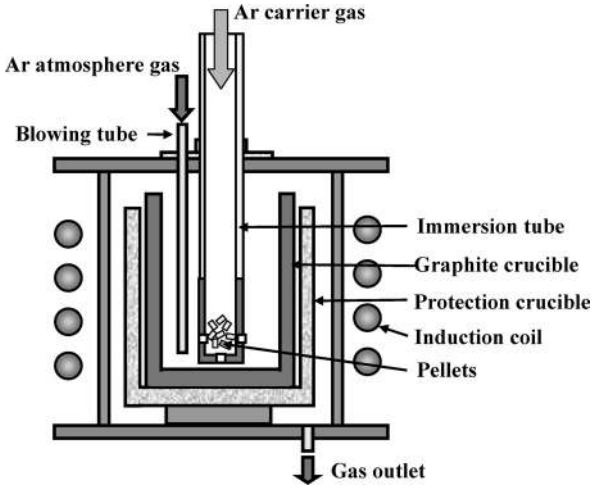

Fig. 1. Experimental apparatus.

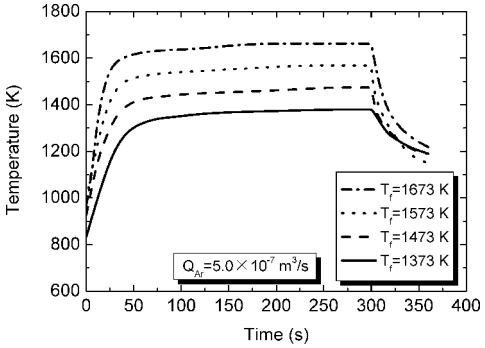

Fig. 2. Changes in temperature with time during descent and ascent of insertion tube.

2. Experimental Apparatus and Procedures

Figure 1 schematically shows the experimental apparatus. A high frequency induction furnace (15 kW, 100 kHz) was used to heat a graphite crucible of 40 mm I.D. and 100 mm in height, in which a high temperature isothermal zone was maintained. The inert atmosphere was maintained by blowing argon gas at a flow rate of 1.3×10^{-5} Nm^3/s into the graphite crucible. A graphite tube of 11 mm I.D., 15 mm O.D. and 60 mm in height had 5 holes of 1.0 mm diameter at its lower part, through which the produced CO and CO_2 gases, and the argon carrier gas flew out. The temperatures in the tube and the crucible were measured with W·5%Re–W·26%Re thermocouples.

The pellets of 0.50 ∓ 0.01 g charged into the graphite tube were composed of hematite powder (less than 10 μm in diameter and purity of 99.9%) and graphite powder (20.3 or 29.2 μm in average diameter and purity higher than 98.0%) with a molar ratio of 1 : 3. Then the pellets were formed by use of a cold isostatic press (CIP) under a pressure of 150 MPa for 1 h, having a diameter of 3 mm and a length of 5 mm. Since the pellet mass is quite limited, the change in temperature caused by the reactions in the pellet can be neglected.

In the present experiment, the isothermal reduction method is utilized. After the temperature in the graphite crucible reached the experimental one and was kept stable, the graphite tube of the good heat conductivity charged with the pellets was promptly inserted into the graphite crucible, in which the high temperature zone was established, to start the reduction. After the reduction experiment, the insertion tube was rapidly lifted up from the crucible to the low temperature zone in the upper part of the furnace to end reduction.

The changes in temperature inside the graphite tube during lowering into and lifting up from the crucible were measured in advance to justify the experimental method of the isothermal reduction. **Figure 2** represents the changes in temperature with time during descent and ascent of the tube for the different experimental temperatures (T_f). The carrier gas flow rate was 5.0×10^{-7} Nm^3/s. The increase in temperature during lowering the tube was very fast. The times needed from inserting the tube to reaching the temperature of T_f-50 (K) were 62, 56, 50 and 42 s for the experimental temperatures of 1 373, 1 473, 1 573 and 1 673 K, respectively. During lifting up the tube, the decrease in temperature was also very quick, being more than 200 K within 60 s at all of the above experimental temperatures. The rapid increase and decrease in temperature inside the tube well satisfied the requirement for the isothermal reduction experiment. Moreover, the effect of the carrier gas flow rate on the rate of temperature change during descent and ascent of the tube was also studied at the temperature of 1 573 K. No obvious difference in the rate of temperature change was observed for the carrier gas flow rates of 0, 5.0×10^{-7} and 3.3×10^{-6} Nm^3/s.

The change in pellet mass during the reduction was measured by using an electronic balance with a detection

precision of 0.1 mg. The reduced pellets were observed using scanning electron microscope (SEM) and optical microscope, and were smashed into powders for XRD analysis using the Cu(K_α) target.

The reactions in the hematite–carbon composite pellets are classified as direct reductions and indirect reductions. The indirect reductions are $3Fe_2O_3+CO=2Fe_3O_4+CO_2$ (1), $Fe_3O_4+CO=3FeO+CO_2$ (2), $FeO+CO=Fe+CO_2$ (3), accompanied by the carbon solution loss reaction of $C+CO_2=2CO$ (4). The direct reductions are $3Fe_2O_3+C=2Fe_3O_4+CO$ (5), $Fe_3O_4+C=3FeO+CO$ (6), $FeO+C=Fe+CO$ (7), and the reduction of wustite by the dissolved carbon of $FeO+[C]=Fe+CO$ (8), accompanied by the carburization reaction of $C=[C]$ (9). With the assumption that the total amount of reduction of iron oxides by CO is equal to the amount of the carbon solution loss reaction, the overall reduction can be expressed as $Fe_2O_3+3C=Fe+3CO$ (10).

Since the molar ratio of Fe_2O_3 to C in the present hematite–graphite composite pellets is 1 : 3, the reduction degree, η_R, can be defined as the ratio of the pellet mass loss to the theoretical pellet mass loss on the assumption that the Reaction (10) is completed. Thus the reduction degree is given by

$$\eta_R = \frac{W_0 - W_f}{W_0 \times \dfrac{3M_{CO}}{M_{Fe_2O_3} + 3M_C}} \times 100\% \quad \text{.....(11)}$$

where W_0 is the pellet mass before reduction (g), W_f is the pellet mass after reduction (g), M is the molecular mass (g/mol).

3. Results and Discussion

3.1. Effect of Temperature on Carbothermal Reduction of Hematite

Figure 3 shows the changes in the reduction degree of iron oxide with time at different temperatures. The carrier gas flow rate is commonly 5.0×10^{-7} Nm^3/s.

The time dependence of the reduction degree at 1 323 K represents the typical reduction behavior of the hematite–graphite composite pellets. The curve consists of three stages. The reduction at the initial stage proceeded relative slowly, and the final reduction degree of the initial stage was 15–23%. At the second stage, the reduction rate was very fast, and the final reduction degree of the second stage reached about 90%. At the third stage, the reduction proceeded rather slowly. In the previous study conducted by Iguchi *et al.*,[10] the iron oxide–graphite composite pellets showed the similar reduction behavior in vacuum.

At the temperature of 1 473 K, the reduction of iron oxide proceeded very fast. In just 120 s, the reduction degree reached 87.6% and the final reduction degree was 92.1%. The pellet mass loss is close to the theoretical pellet mass loss according to Reaction (10). Therefore, the assumption of Reaction (10) that the total amount of reduction of iron oxides by CO is equal to the amount of the carbon solution loss reaction is essentially valid. When the temperature was decreased to 1 373 K, the initial reduction rate was slightly decreased, but the final reduction degree slightly increased to 94.3%. When the temperature was further decreased to 1 323 K, the initial reduction rate was greatly decreased, but from 720 to 900 s, the reduction rate was remarkably fast, the reduction degree increased sharply from 25.0 to 92.5%. The final reduction degree further increased to 95.8%. When the temperature was 1 273 and 1 173 K, the reduction degree increased to 9.9 and 8.6% at 600 s, 12.2 and 9.4% at 1 800 s. The reduction proceeded rather slowly.

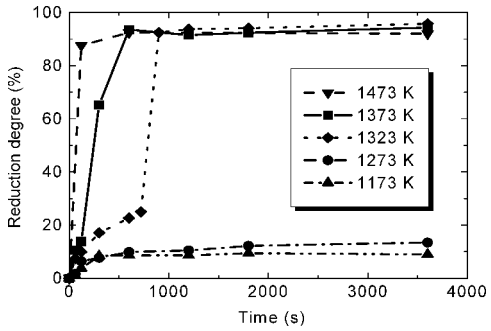

Fig. 3. Effect of temperature on reduction rate of hematite.

At the temperatures of 1 323 and 1 473 K, the morphological changes of pellets are given in **Fig. 4**. With the progress of reduction, owing to the release of the CO and CO_2 gases, the pellet shrank. At the end of the experiment at 1 473 K, the pellet was in globular shape. This is because the reduced iron melted down due to the decrease in its melting point caused by carburization. Therefore, the difference between the theoretical and the final reduction degrees is caused by the lack of carbon due to the carburization of iron, because the amount of graphite was stoichiometrically added according to Reaction (10). The reason that the final reduction degrees decrease in the sequence of 1 323, 1 373 and 1 473 K is that the carburization is enhanced at a higher temperature.

Figure 5 presents the morphological changes in pellet by observation with SEM. The magnification was 2 000 times, the temperature was 1 373 K, the carrier gas flow rate was 5.0×10^{-7} Nm^3/s. Before reduction, the graphite particles had the diameter of about 30 μm and could be clearly distinguished by microphotograph. The Fe_2O_3 particles were very fine, and most of them had the diameter of several micrometers.

With the reduction progress, the graphite particles became smaller, and the surface of graphite particles was covered by the reduction products, which would break the contact between the hematite and the graphite particles. Therefore, after the reduction proceeded for a certain time, the direct reduction caused by the contact between the hematite and the graphite particles was not liable to take place. The indirect reduction and the carbon solution loss reaction should dominate the reduction rate.

After 600 s, the graphite particles could not be distinguished by microphotograph because they were almost consumed by the reduction of iron oxide due to the reduction degree of 94%. There were a lot of voids in the produced iron as shown in the pictures after 600 s. This indicates that the reduced iron was in a shape of sponge at the relatively low temperature.

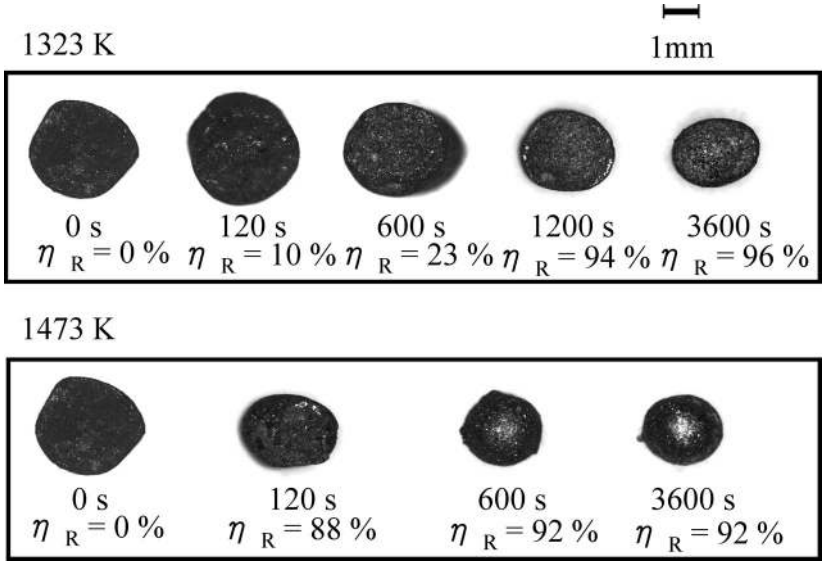

Fig. 4. Observation of pellets at different reduction stages at 1 323 and 1 473 K.

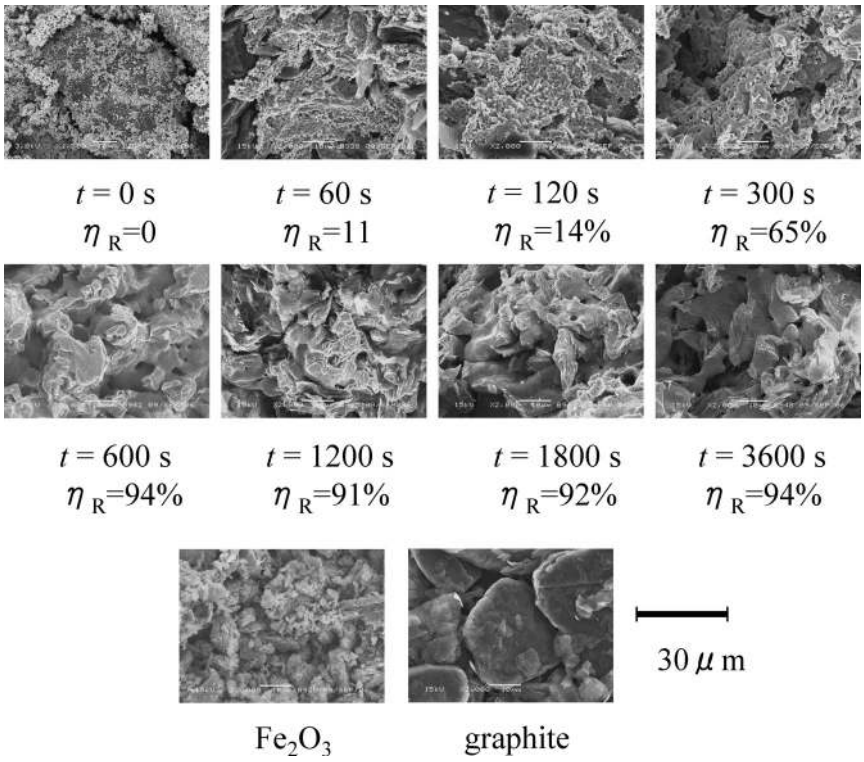

Fig. 5. SEM observation of pellets at different reduction stages at 1 373 K.

For the carbothermic reduction of iron oxide, it is widely accepted that the overall reaction rate is controlled by the carbon solution loss Reaction (4) at below about 1 373 K.[28] Therefore, the very slow reduction rates at 1 173 and 1 273 K are due to the rather slow rate of the carbon solution loss Reaction (4) at these temperatures. The reduction mainly proceeds in the direct reduction, and the indirect reduction is not liable to take place because of the very low CO partial pressure. At the initial stages at the temperatures of 1 323 and 1 373 K, the reduction also mainly proceeds in the direct reduction to produce CO. After the CO partial pressure exceeds a certain value that is determined by the reduction temperature, the indirect reduction begins to take place from 720 s at 1 323 K, and from 120 s at 1 373 K. At these stages, the occurrence of the indirect reduction is also supported by the SEM observation of reduced pellets at different reduction stages as stated above. The produced CO_2 by the indirect reduction reversely reacts with C to produce CO. So, the indirect reduction is further promoted. As a result, the overall reduction can be written in Reaction (10). It is an apparent direct reduction. In this way, the reduction degree increases very fast. When the temperature was further increased to 1 473 K, the stagnant stage of initial reduction did not appear. This means that the indirect reduction together with the carbon solution loss reaction began at the very initial stage of reduction.

In the present experiment, because the distance between the graphite and the iron oxide particles is extremely close

to each other, the contact area between the graphite and the iron oxide particles is greatly increased. Furthermore, since the heat conduction rate through solid particles is much faster than that through the voids in the reaction materials, the direct reduction, which is endothermic reaction, is greatly promoted and CO gas is produced. After a certain CO partial pressure is reached, the indirect reduction begins to take place to produce CO_2 gas. And then the carbon solution loss reaction can take place. The indirect reduction is much faster than the direct reduction due to its gas–solid reaction. As a result, the carbothermic reduction of hematite is greatly enhanced in the present hematite–graphite composite pellets made by CIP. The beginning temperature for activation of the indirect reduction and the carbon solution loss reaction decreases to 1 323 K.

3.2. Clarification of Reduction Behavior Based on XRD Patterns of Pellets

To clarify the mechanism of the carbothermic reduction of hematite, the pellets at different reduction stages were analyzed with XRD and the results are shown in **Fig. 6**. The reduction experiment was carried out under the conditions of a temperature of 1 373 K and a carrier gas flow rate of 5.0×10^{-7} Nm^3/s.

Before reduction, the XRD pattern shows that the pellets contained hematite and carbon. The strongest peak of the XRD pattern appeared for the crystal plane (104) with the diffraction angle of $2\theta=42.04°$ for hematite, and for the crystal plane (002) with the diffraction angle of $2\theta=33.54°$ for graphite. It is clear that with the reduction progress, the intensities of the graphite and Fe_2O_3 peaks decreased, while the peaks of Fe_3O_4, FeO and Fe appeared in turn.

The temporal changes in the intensities of the peaks of Fe_2O_3(104), Fe_3O_4(511), FeO(200) and Fe(110) are presented in **Fig. 7**. The intensity of the peak of hematite decreased rapidly with the reduction proceeding, and disappeared at 60 s. The intensity of the peak of magnetite increased at first, reached the maximum value at 60 s, and then decreased. Its peak disappeared at 300 s. The peak of wustite increased from 60 s, while the peak of iron rose from 120 s. These results clearly show the progress of carbothermic reduction of hematite at 1 373 K. When hematite was reduced, magnetite was produced until 60 s. Magnetite was then reduced to produce wustite until 300 s. After 120 s, wustite was reduced and metallic iron was produced.

With the similar method, the changes in the intensities of the peaks of Fe_2O_3(104), Fe_3O_4(511), FeO(200) and Fe(110) with time are shown in **Fig. 8** for 1 323 K, in **Fig. 9** for 1 273 K, and in **Fig. 10** for 1 173 K. For the different temperatures, the carbothermic reduction of hematite proceeded in the same sequence as that described above. But with the temperature decreased, it took a longer time for the changes in reductions of from hematite to magnetite, and from magnetite to wustite. At the temperature below 1 273 K, no metallic iron was detected in the reduction products.

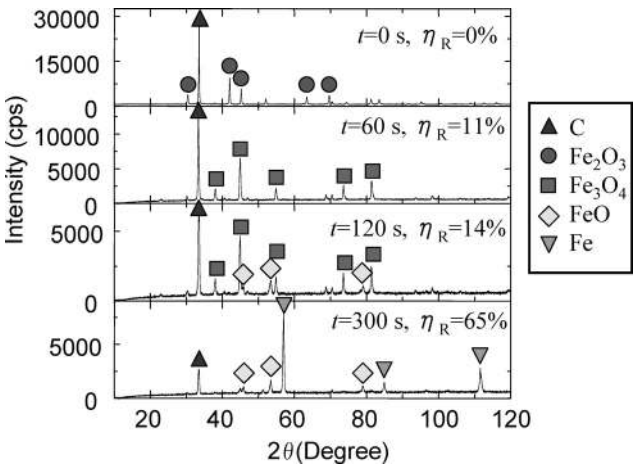

Fig. 6. XRD patterns of pellets at different reduction stages at 1 373 K.

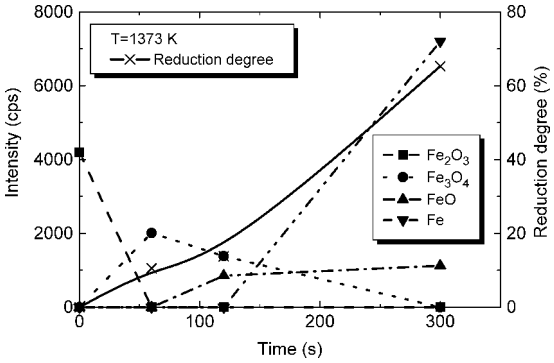

Fig. 7. Variation of intensities of peaks of Fe_2O_3(104), Fe_3O_4(511), FeO(200) and Fe(110) in XRD patterns with time at 1 373 K.

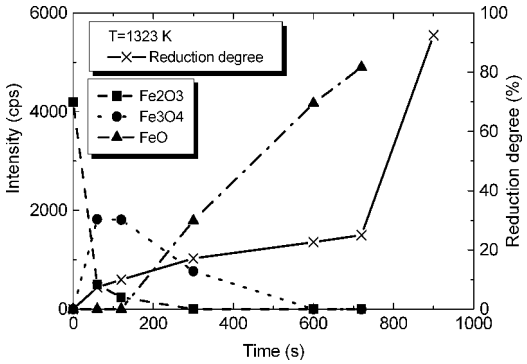

Fig. 8. Variation of intensities of peaks of Fe_2O_3(104), Fe_3O_4(511) and FeO(200) in XRD patterns with time at 1 323 K.

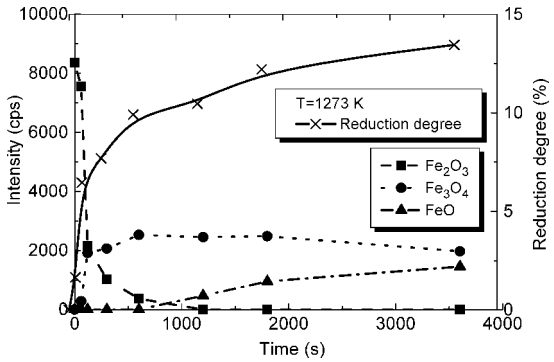

Fig. 9. Variation of intensities of peaks of Fe_2O_3(104), Fe_3O_4(511) and FeO(200) in XRD patterns with time at 1 273 K.

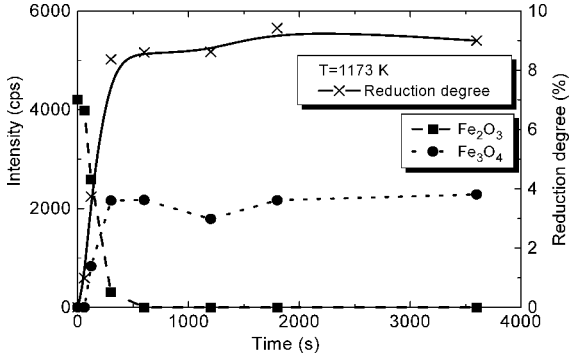

Fig. 10. Variation of intensities of peaks of Fe_2O_3(104) and Fe_3O_4(511) in XRD patterns with time at 1 173 K.

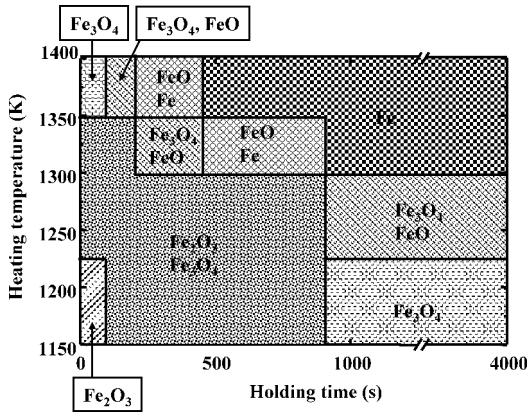

Fig. 11. Relationship of reduction products, heating temperature and holding time during carbothermic reduction of hematite.

Therefore, from the above XRD analysis results, the relationship of reduction products, heating temperature and holding time during carbothermic reduction of hematite under the present experimental conditions can be roughly summarized in **Fig. 11**. It is seen that the reduction products changes with both temperature and time. For example, at the reduction time of 1 000 s, magnetite is the reduction product below 1 223 K, which is the average value of the experimental temperatures of 1 173 and 1 273 K. The heating temperature and holding time used for dividing the regions of reduction products are obtained in the same method hereinafter. Magnetite and wustite are the reduction products from 1 223 to 1 298 K, and metallic iron is the reduction product above 1 298 K. At the temperature of 1 273 K, hematite and magnetite are the reduction products before 900 s, and magnetite and wustite are the reduction products after 900 s.

3.3. Effect of Carrier Gas Flow Rate on Carbothermic Reduction of Hematite

At the temperature of 1 323 K, the effect of carrier gas flow rate on carbothermic reduction of hematite is given in **Fig. 12**. Since 0.5 g pellets of Fe_2O_3 and C at the molar ratio of 1 : 3 was used, with the assumption that Reaction (10) proceeds at a constant rate and finishes in about 1 000 s, the generation rate of CO will be 1.7×10^{-7} Nm^3/s. For the Ar carrier gas flow rate of 5.0×10^{-7} Nm^3/s, the average CO partial pressure will be 0.25 atm, while for the Ar carrier gas flow rate of 3.3×10^{-6} Nm^3/s, the average CO partial pressure will be 0.05 atm. At the carrier gas flow rate of 5.0×10^{-7} Nm^3/s, the reduction rate was the fastest. At the carrier gas flow rates of 0 and 3.3×10^{-6} Nm^3/s, the reduction rate was decreased.

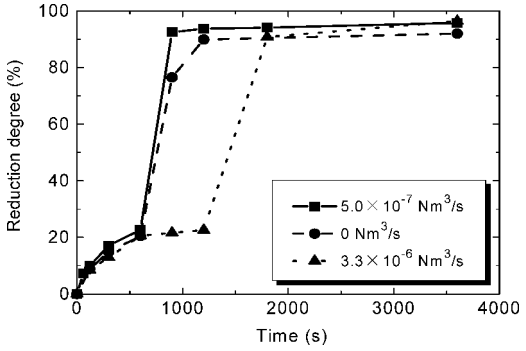

Fig. 12. Effect of carrier gas flow rate on reduction rate of hematite.

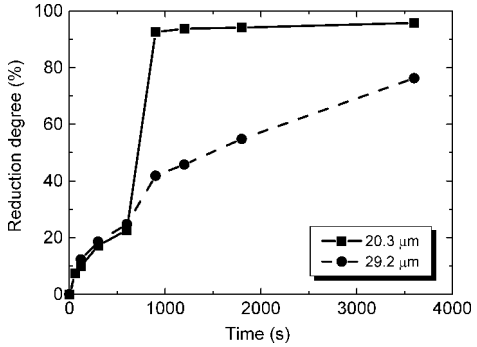

Fig. 13. Effect of graphite particle size on reduction rate of hematite.

Without the carrier gas, since the produced CO gas is difficult to be removed from the reaction site, the direct reductions of Reactions (5), (6) and (7) are somewhat inhibited. When the carrier gas flow rate is as large as 3.3×10^{-6} Nm^3/s, the CO partial pressure is obviously decreased, the beginning of indirect reduction is markedly retarded from 600 s to 1 200 s, and its reduction rate is also decreased.

3.4. Effect of Graphite Particle Size on Carbothermic Reduction of Hematite

Under the experimental conditions of a temperature of 1 323 K, and a carrier gas flow rate of 5.0×10^{-7} Nm^3/s, the effect of graphite particle size on carbothermic reduction rate of hematite is given in **Fig. 13**. With the average graphite particle diameter increased from 20.3 to 29.2 μm, the reduction rate was greatly decreased.

For simplicity, the specific surface area of graphite particles (A, m^2/kg) can be calculated as $A=n\cdot\pi d_{av}^2$, where d_{av} is the average diameter of particles (m), n is the particle number per unit mass (kg^{-1}), which can be written as $n=6/(\rho\pi d_{av}^3)$, where ρ is the real particle density (kg/m^3). Therefore, $A=6/(\rho d_{av})$. Namely, the specific surface area of graphite particles is inversely proportional to the average diameter of particles.

In the present case, with decreasing the average diameter from 29.2 to 20.3 μm, the specific surface area increases by 1.44 times. As a result, the carbon solution loss reaction is greatly promoted, and the reduction rate becomes faster.

The significant enhancement of reduction rate by decreasing the graphite particle size also indicates that the carbon solution loss reaction is one of the rate controlling steps at the temperature of 1 323 K.

4. Conclusions

Isothermal reduction experiments were carried out to study the carbothermic reduction rate of hematite in hematite–graphite composite pellets, which were charged into an insertion tube. Effects of temperature, carrier gas flow rate and graphite particle size on the carbothermic reduction rate of hematite were investigated. To clarify the reduction mechanism, XRD analyses of the pellets at different reduction stages for various temperatures were carried out, and SEM observations of the reduced pellets were conducted. The following conclusions can be drawn:

(1) The rapid increase in temperature during lowering the tube into a high temperature zone and the fast decrease in temperature during lifting up the tube to a low temperature zone indicates that the isothermal condition of the carbothermic reduction of hematite can be essentially satisfied.

(2) The initial stage of carbothermic reduction of hematite is dominated by the direct reduction. At the higher temperature, after the CO partial pressure exceeds a certain value, the indirect reduction together with the carbon solution loss reaction will take place. The cabothermic reduction of hematite is greatly promoted because the contact area between the graphite and the iron oxide particles is remarkably increased, and the heat conduction is greatly promoted in the hematite–graphite composite pellet made by CIP.

(3) Since increasing temperature can greatly activate the indirect reduction and the carbon solution loss reaction, the cabothermic reduction of hematite is greatly promoted. The carbothermic reduction rate reaches the highest value at a moderate carrier gas flow rate. Decreasing graphite particle size can effectively enhance reduction rate due to promotion of the carbon solution loss reaction.

(4) From the SEM observation of the reduced pellets, the graphite particles are covered with reduction products after a certain reduction time. Therefore, the indirect reduction together with the carbon solution loss reaction should dominate the carbothermic reduction at the later stage of reduction.

(5) From the XRD patterns at the different stages for various temperatures, the relationship of reduction products, heating temperature and holding time has been obtained under the present experimental conditions.

REFERENCES

1) F. N. Griscom and D. R. Lyles: *Steel Times*, **222** (1994), 491.
2) R. Munnix, J. Borlee, D. Steyls and M. Economopoulos: *MPT Int.*, **2** (1997), 50.
3) Y. Sawa, T. Yamamoto, K. Takeda and H. Itaya: *ISIJ Int.*, **41** (2001), S17.
4) Y. Matsui, M. Sawayama, A. Kasai, Y. Yamagata and F. Noma: *ISIJ Int.*, **43** (2003), 1904.
5) C. Kamijo, M. Hoshi, T. Kawaguchi, H. Yamaoka and Y. Kamei: *ISIJ Int.*, **41** (2001), S13.
6) M. Nakano, M. Naito, K. Higuchi and K. Morimoto: *ISIJ Int.*, **44** (2004), 2079.
7) Y. Kashiwaya, M. Kanbe and K. Ishii: *ISIJ Int.*, **41** (2001), 818.
8) Y. Iguchi: *Tetsu-to-Hagané*, **85** (1999), 447.
9) Y. Iguchi and R. Kamei: *Tetsu-to-Hagané*, **85** (1999), 439.
10) Y. Iguchi and Y. Takada: *ISIJ Int.*, **44** (2004), 673.
11) Y. Iguchi and S. Yokomoto: *ISIJ Int.*, **44** (2004), 2008.
12) T. Matsumura, Y. Takenaka, M. Shimuzu, T. Negami, I. Kobayashi and A. Uragami: *Tetsu-to-Hagané*, **84** (1998), 405.
13) T. Yamamoto, Y. Sawa and K. Takeda: *Tetsu-to-Hagané*, **87** (2001), 734.
14) E. Kasai, T. Kitajima and T. Kawaguchi: *ISIJ Int.*, **40** (2000), 842.
15) F. M. Meng, Y. Iguchi and I. Kojima: *Tetsu-to-Hagané*, **87** (2001), 585.
16) A. Kasai, M. Naito, Y. Matsui and Y. Yamagata: *Tetsu-to-Hagané*, **89** (2003), 1212.
17) T. Matsumura, Y. Takenaka and M. Shimizu: *Tetsu-to-Hagané*, **85** (1999), 652.
18) Y. Ueki, T. Maeda, M. Shimizu, Y. Matsui and A. Kasai: *Tetsu-to-Hagané*, **89** (2003), 1205.
19) A. Kasai, Y. Matsui, F. Noma, H. Iwakiri and M. Shimizu: *Tetsu-to-Hagané*, **87** (2001), 313.
20) K. Nagata, R. Kojima, T. Murakami, M. Susa and H. Fukuyama: *ISIJ Int.*, **41** (2001), 1316.
21) K. Ishizaki, K. Nagata and T. Hayashi: *ISIJ Int.*, **46** (2006), 1403.
22) E. Kasai, K. Mae and F. Saito: *ISIJ Int.*, **35** (1995), 1444.
23) J. V. Khaki, Y. Kashiwaya, K. Ishii and H. Suzuki: *ISIJ Int.*, **42** (2002), 13.
24) Y. Kashiwaya, H. Suzuki and K. Ishii: *ISIJ Int.*, **44** (2004), 1970.
25) Y. Kashiwaya, H. Suzuki and K. Ishii: *ISIJ Int.*, **44** (2004), 1975.
26) Y. Kashiwaya and K. Ishii: *ISIJ Int.*, **44** (2004), 1981.
27) I. Seki and K. Nagata: *ISIJ Int.*, **46** (2006), 1.
28) R. J. Fruehan: *Metall. Trans. B*, **8B** (1977), 279.